REPORT DOCUMENTATION PAGE

Form Approved
OMB No. 0704-0188

1. REPORT DATE *(DD-MM-YYYY)*	2. REPORT TYPE	3. DATES COVERED *(From - To)*
04/03/2017	Final	July 2012 - September 2016

4. TITLE AND SUBTITLE
Coupling of Coastal Wave Transformation and Computational Fluid Dynamics Models for Seakeeping Analysis

5a. CONTRACT NUMBER

5b. GRANT NUMBER
N00014-12-1-0721

5c. PROGRAM ELEMENT NUMBER

6. AUTHOR(S)
Cheung, Kwok Fai

5d. PROJECT NUMBER

5e. TASK NUMBER

5f. WORK UNIT NUMBER

7. PERFORMING ORGANIZATION NAME(S) AND ADDRESS(ES)
Department of Ocean and Resources Engineering
University of Hawaii at Manoa
2540 Dole Street, Holmes Hall 402
Honolulu, Hawaii 96822

8. PERFORMING ORGANIZATION REPORT NUMBER

9. SPONSORING/MONITORING AGENCY NAME(S) AND ADDRESS(ES)
Office of Naval Research
One Liberty Center
875 North Randolph Street
Arlington, VA 22203-1995

10. SPONSOR/MONITOR'S ACRONYM(S)
ONR

11. SPONSOR/MONITOR'S REPORT NUMBER(S)

12. DISTRIBUTION/AVAILABILITY STATEMENT
Approved for public release; distribution unlimited

13. SUPPLEMENTARY NOTES

14. ABSTRACT
The project focused on depth-integrated modeling of coastal wave and surf-zone processes in support of computational fluid dynamics (CFD) simulation of ship motions. There were two components of the project involving two MS and one PhD candidate under the guidance of the principal investigator. The first was the development of a numerical dispersion relation for a family of Boussinesq-type equations commonly used in modeling of coastal wave transformation and the second was an extension of existing depth-integration models to describe overtopping of coastal reefs and structures along with series of CFD and laboratory experiments for model validation.

15. SUBJECT TERMS
Coastal wave modeling, dispersion relation, wave overtopping

16. SECURITY CLASSIFICATION OF:			17. LIMITATION OF ABSTRACT	18. NUMBER OF PAGES	19a. NAME OF RESPONSIBLE PERSON
a. REPORT	b. ABSTRACT	c. THIS PAGE			Kwok Fai Cheung
					19b. TELEPHONE NUMBER *(Include area code)*
U	U	U	UU	12	(808) 956-3485

Final Report

Submitted to the Office of Naval Research

Award Number: N00014-12-1-0721

Project Title: Coupling of Coastal Wave Transformation and Computational Fluid Dynamics Models for Seakeeping Analysis

Awardee: University of Hawaii, Honolulu, Hawaii

Technical Contact: Kwok Fai Cheung, PhD, PE
Professor and Graduate Chair
Department of Ocean and Resources Engineering
University of Hawaii at Manoa
2540 Dole Street, Holmes Hall 402
Honolulu, Hawaii 96822
Phone: (808) 956-3485
Fax: (808) 956-3498
Email: cheung@hawaii.edu

Administrative Contact: Kathleen S. Yoshinaga
Grants Specialist
Office of Research Services
University of Hawaii
2440 Campus Road, Box 368
Honolulu, Hawaii 96822
Phone: (808) 956-7800
Fax: (808) 956-9081
Email: kyoshina@hawaii.edu

Duration of Effort: July 1, 2012 – September 30, 2016

Report Date: April 3, 2017

EXECUTIVE SUMMARY

The project focused on depth-integrated modeling of coastal wave and surf-zone processes in support of computational fluid dynamics (CFD) simulation of ship motions. There were two components of the project involving two MS and one PhD candidate under the guidance of the principal investigator. The first was the development of a numerical dispersion relation for a family of Boussinesq-type equations commonly used in modeling of coastal wave transformation. The relation depicts numerical dissipation and dispersion in wave propagation and provides guidelines for model setup in terms of temporal and spatial discretization. The second component was an extension of existing depth-integrated wave models to describe overtopping of coastal reefs and structures along with series of CFD and laboratory experiments for model validation. The basic approach utilizing the HLLS Riemann solver performs reasonably well and produces stable and efficient numerical results for practical application. Although the two components were performed separately, they both contribute to improved capabilities in modeling of the coastal wave environment that can provide input to three-dimensional seakeeping analysis.

TABLE OF CONTENTS

1. Introduction

Seakeeping analysis has traditionally been focused on dynamic response of vessels in the open ocean. As the attention is shifted to the littoral, a capability gap becomes obvious in the naval research and ship design communities. The distinct wave processes in the coastal region result in vessel loads and motions that are significantly different from those in the open ocean. Recent advances in depth-integrated models have enabled computations of wave transformation from the open ocean to the coast to provide important information for seakeeping analysis. However, such endeavors involve appreciable numerical errors and complex near-shore flows that might present a challenge to practical application.

Most coastal wave models are based on finite difference solution of Boussinesq-type equations. The depth-integrated governing equations express the vertical flow structure in terms of high-order spatial derivatives of the horizontal velocity through the irrotational flow condition (Peregrine, 1967). Subsequent developments have improved the dispersion and nonlinear properties, but greatly increased the complexity of the governing equations (e.g., Madsen et al., 1991; Nwogu, 1993; Wei et al., 1995; Madsen and Schäffer, 1998; Gobbi et al., 2000; Fuhrman and Madsen, 2009). Since the depth-integrated formulation cannot handle an overturning free surface, these early Boussinesq-type models typically utilized an empirical approach to approximate energy dissipation due to wave breaking. Roeber et al. (2010) and Roeber and Cheung (2012) introduced a shock-capturing scheme for modeling of breaking waves as flow discontinuities and validated their model with laboratory experiments conducted at Oregon State University.

Following the exponential growth of computing resources and parallel pursuit of highly nonlinear and dispersive theories, present-day computational models based on Boussinesq-type equations are being applied over vast regions from deep to shallow water with increasing resolution. The computational scheme, however, does not explicitly solve the governing system of partial differential equations (Abbott, 1976). Discretization schemes involve numerical dispersion and dissipation that distort the true character of the governing equations. The leading term in the truncation error contains a derivative of the same order as the dispersion terms in Boussinesq-type equations. Such numerical errors have been studied extensively for the shallow-water equations (Imamura et al., 1988; Yoon et al., 2007; Wang and Liu, 2011), which represent a leading-order approximation of the Boussinesq-type equations. Tam and Webb (1993) proposed a wavenumber-based discretization scheme to preserve the dispersion relation of the governing equations, but there has been no research on the effects of numerical dispersion in Boussinesq-type equations and the resulting wave propagation characteristics.

Overtopping on coastal reefs or structures becomes an importance process as modeling of wave transformation extends into the nearshore region. George (2008) included effects of a bottom step as a forcing or source term in the Riemann problem and derived an approximate solver for the augmented system. The resulting model reproduces field and laboratory measurements of dam-break flows over rugged mountain terrain (George, 2011). Murillo and Garcia-Navarro (2010, 2012) generalized the effects of the bottom step as a hydrostatic force on the flow. Implementation of the resulting solver, known as HLLS (S for step), in one and two-dimensional nonlinear shallow-water models produces good agreement with analytical solutions and laboratory measurements. Application of these Riemann solvers has so far been limited to

stepwise approximation of irregular topography for conservation of the hyperbolic flow character. Although these solvers do not include vertical flows to physically describe overtopping, they can better approximate the resulting characteristic flows for modeling of coastal wave processes.

The project aimed to improve the fidelity of coastal wave modeling in support of seakeeping analysis. The efforts included development of a numerical dispersion relation for the Boussinesq-type equations using the spectral method of Tam and Webb (1993) and extension of the capability to describe wave overtopping using the HLLS Riemann solver of Murillo and Garcia-Navarro (2010, 2012). Two MS and one PhD candidate worked on the project under the guidance of the principal investigator. This report provides a synopsis of their research and development work. More detailed description of the project can be found in their theses and publications (Heitmann et al., 2015; Stephenson, 2015; Wesley, 2015; and Wesley and Cheung, 2016).

2. Numerical Dispersion Relation

Let t and x denote time and space for the depth-integrated wave propagation problem. The Boussinesq-type equations can be written in the matrix form as

$$\mathbf{U}_t + \mathbf{F}(\mathbf{U})_x = \mathbf{S}(\mathbf{U}) \tag{11}$$

where **U** is the vector of conserved variables, **F**(**U**) is the flux vector, and **S**(**U**) contains the source and dispersion terms. The governing system of partial differential equations is modified through its discretization, providing a family of solutions dependent upon the sampling intervals Δx and Δt in time and space as well as the numerical scheme. We focus on the solution of a semi-implicit scheme composed of linear multi-step time integration and spatial central difference, which collectively preserve the frequency dispersion relation intrinsic to the partial differential equations (Webb and Tam, 1993).

Applying Fourier-Laplace transforms to the discrete approximation of the governing equation (1), the system of modified partial differential equations is mapped into spectral space in terms of the angular frequency ω and wave number k for derivation of the numerical dispersion relation:

$$\omega^2 \left(\frac{\bar{\omega}\Delta t}{\omega \Delta t}\right)^2 = ghk^2 \left(\frac{\bar{k}_1 \Delta x}{k\Delta x}\right)^2 \left[1 - \alpha_1 (kh)^2 \left(\frac{\bar{k}_3 \Delta x}{k\Delta x}\right)^3 \left(\frac{k\Delta x}{\bar{k}_1 \Delta x}\right)\right] \left[1 - \alpha (kh)^2 \left(\frac{\bar{k}_2 \Delta x}{k\Delta x}\right)^2\right]^{-1} \tag{22}$$

where h is water depth, g is gravitational acceleration, α and α_1 are dispersion coefficients, and $\bar{\omega}$ and $\bar{k}_n$ are the frequency and wave number resolved by the numerical scheme. The relation defines the dispersion and dissipation characteristics of the numerical model in terms of Δx and Δt. The effective resolutions $\bar{\omega}\Delta$t and $\bar{k}_n \Delta x$ are obtained from Laplace and Fourier transforms of the time integration and spatial discretization schemes. If the physical resolutions $\omega\Delta t$ and $k\Delta x$ are identical to the effective resolutions, the numerical dispersion relation reduces to

$$\omega^2 = ghk^2 \left[\frac{1-\alpha_1 (kh)^2}{1-\alpha (kh)^2}\right] \tag{33}$$

which is the dispersion relation of the governing equations. Setting α = -0.39 and α_1 = α+1/3 recovers the Boussinesq-type equations of Nwogu (1993) for demonstration here.

Introducing the dimensionless parameter $h/\Delta x$ in the numerical dispersion relation (2) allows direct comparison of the wave propagation characteristics of the modified and original partial differential equations. Figure 1 plots the errors of the numerical celerity $\bar{c}$ in relation to Airy wave theory. Modelers can identify the spatial interval Δx to achieve an acceptable level of convergence for a given water depth parameter kh. The same information can also be used to offset theoretical limitations of the governing equations through discretization errors.

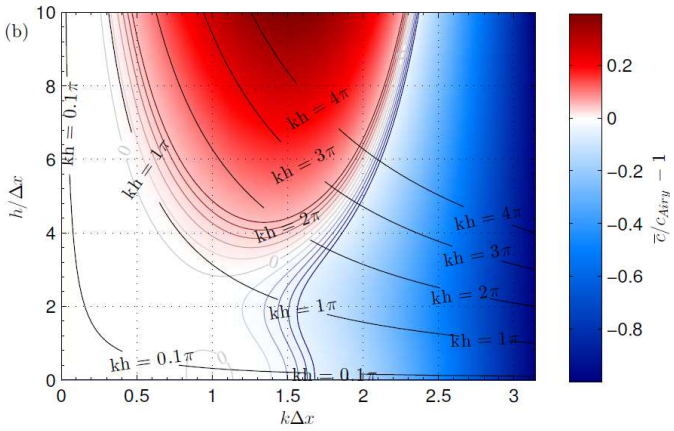

Figure 1. Relative errors of numerical celerity in relation to Airy wave theory.

The effective resolutions $\bar{\omega}\Delta t$ and $\bar{k}_n\Delta x$ are determined from the discretization scheme, thereby providing important metrics for its performance. Reducing the formal order of accuracy in the scheme introduces additional degrees of freedom, which permit optimization of spectral properties at the expense of bounded oscillatory errors in the low-frequency range (Tam and Webb, 1993). Research in this area is still on-going at the University of Hawaii. A series of computational experiments are being conducted to verify the numerical dispersion relation, including an analysis of the subtle oscillatory features from the optimization and the phase shift associated with the original and modified partial differential equations.

3. Modeling of Wave Overtopping

Depth-integrated wave models provide an effective tool to describe near-shore processes, but the results might be unstable or questionable when overtopping of coastal reefs and structures is involved. The HLLS Riemann solver presented by Murillo and Garcia-Navarro (2010, 2012) can account for shallow-water flow across a bottom step. Omitting dispersion in the governing equation (1), the Riemann problem consists of a hyperbolic system with two constant states separated by an initial surface discontinuity over the bottom step as illustrated in Figure 2. In the analytical solver, the step imposes a hydrostatic force on the flow maintaining the local surface discontinuity and waves propagate away in the form of a shock or rarefaction. The HLLS Riemann solver can uniquely define the middle-state fluxes on the two sides of the step. Application of the solver had been limited to stepwise approximation of irregular topography for conservation of the hyperbolic flow character. The project demonstrated for the first time its potential to describe overtopping and the resulting characteristic flows.

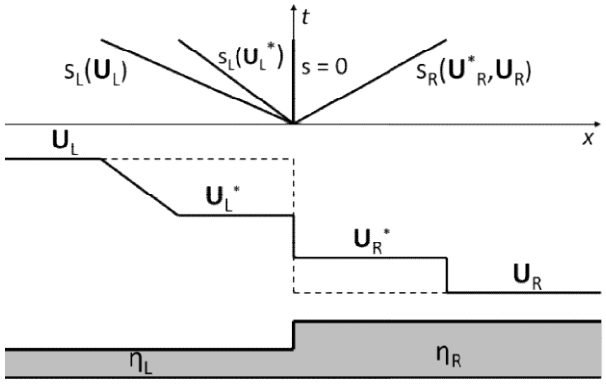

Figure 2. Illustration of the HLLS Riemann problem and solver. The subscripts L and R indicate the characteristic flows on the left and right sides of the bottom step.

We implemented the HLLS Riemann solver in a second-order MUSCL-Hancock scheme as a proof-of-concept. The scheme involves time integration of the conserved variables from the governing equation (1) through a predictor and a corrector step as

$$\mathbf{U}_i^{n+\frac{1}{2}} = \mathbf{U}_i^n - \frac{\Delta t}{2\,\Delta x}\left[\left((\mathbf{F}_L)_{i+\frac{1}{2}}^n - (\mathbf{F}_R)_{i-\frac{1}{2}}^n\right) - \mathbf{S}_i^n\right] \tag{4}$$

$$\mathbf{U}_i^{n+1} = \mathbf{U}_i^n - \frac{\Delta t}{\Delta x}\left[\left((\mathbf{F}^-)_{i+\frac{1}{2}}^{n+\frac{1}{2}} - (\mathbf{F}^+)_{i-\frac{1}{2}}^{n+\frac{1}{2}}\right) - \mathbf{S}_i^{n+\frac{1}{2}}\right] \tag{5}$$

where the indices i and $i\pm½$ denote cell center and interface variables and n is the current time step. The predictor step (4) evolves the conserved variables over a half time step based on the flux and source terms at the current time. The predicted variables revise the source term and along with the solver define the fluxes on the left and right sides of the interface, denoted by $\mathbf{F}^-$ and $\mathbf{F}^+$ in equation (5), for update of the flow over a full time step.

This Godunov-type scheme discretizes a conservative system with a series of cells and solves the HLLS Riemann problem at each interface to capture flow discontinuities. Both the predictor and corrector steps involve reconstruction of the interface fluxes from the conserved variables at the cell centers. The second-order scheme defines the variables as piece-wise linear in each cell. The surface-gradient method proposed by Zhou et al. (2001) reconstructs the interface surface elevation instead of the flow depth to eliminate depth-interpolation errors. To reduce spurious oscillations, a slope limiter is applied to remove unrealistic gradients across discontinuities during the variable reconstruction. The minmod limiter, which works well with the present problem, is applied to both the surface elevation and momentum before the computation of the interface fluxes. A bottom step can represent the front or back wall of a vertical structure for modeling of overtopping. Because of the large elevation difference between the adjacent cells, a second-order limiter provides unrealistic reconstructed values at the interface. A first-order limiter with upwind or downwind bias is applied within the cells adjacent to the wall. The use of flow information from the respective side avoids creating an artificial gradient across the step. This local treatment is important for approximation of flows across a large bottom discontinuity and maintaining accuracy and stability of the model results.

4. CFD Experiment

OpenFOAM (Open source Field Operation and Manipulation) is an open-source CFD toolbox that enables customization of applications in continuum mechanics and chemical processes. The InterFOAM solver within OpenFOAM makes use of the volume of fluid (VoF) technique to track the interface of a two-phase flow (Weller et al., 1998). A scalar function defines the ratio of air to water in each computational cell and typically a value of 0.5 delineates the free surface. With sufficient resolution, this technique can resolve splashing and air entrainment to realistically describe the flow field across a large bottom step. This feature is important for validation of the HLLS Riemann solver. The InterFOAM module solves the Navier-Stokes equations for each phase simultaneously. For this application, the fluid viscosity is set to zero. The resulting Euler equations in two dimensions are utilized for consistency with the inviscid fluid assumption in the Riemann problem.

We conducted a series of numerical tests, which include various combinations of the left and right initial states separated by a surface discontinuity over a step as illustrated in Figure 2. Each test case is devised to mimic or isolate an aspect of the Riemann problem for direct comparison with the solution from OpenFOAM. The computational domains correspond to a flume of 60 m long and 2.5 m high with the bottom step at the center. The height of the domain is not a factor in the depth-integrated model and the vertical wall of the step is modeled by the interface of the two adjacent cells. The initial conditions also define the steady upstream boundary conditions on the left side, while a reflective condition is imposed at the downstream boundary. Bed friction is not considered in the depth-integrated model to be consistent with the Riemann problem, while the free slip condition and a zero pressure gradient are applied at all boundaries in OpenFOAM. Sensitivity tests showed a grid size of 0.05 m in the depth-integrated model can accurately capture the shock waves and a grid size of 0.02 m by 0.02 m in OpenFOAM produces converging numerical results for the test cases.

Overtopping of a structure involves a series of hydraulic processes that are fundamental of the characteristic flows embedded in the HLLS Riemann Solver. The incoming flow is partially reflected from the front wall, while developing into a surge on the initially dry crest prior to spilling over the back wall of the structure. Figure 3 compares the results with OpenFOAM for a test case involving the upstream and surge processes. With an initial still-water condition, both models produce a jump at the step and a rarefaction wave propagating to the left as shown in Figure 3a. OpenFOAM shows gradual development of the jump and noticeable modulation of the rarefaction from the transient circulation by the step. Figure 3b illustrates the results with an initial flow velocity toward the step. The depth-integrated model produces a stationary jump at the step as well as a reflected shock wave instantly. The middle state and shock height remain steady throughout the simulation. The sequence of snapshots indicates the jump and reflection from OpenFOAM develop gradually from the incoming flow redirected upward by the step. The jump increases over time reaching the same level as the depth-integrated prediction. The reflected wave subsequently develops into a steady state with a greater height than the shock. The hydrostatic assumption in the HLLS Riemann solver deviates when a circulation develops in front of the step. Despite the discrepancies in the upstream flow, the depth-integrated model gives excellent agreement with OpenFOAM for the surge on the dry bed in both cases.

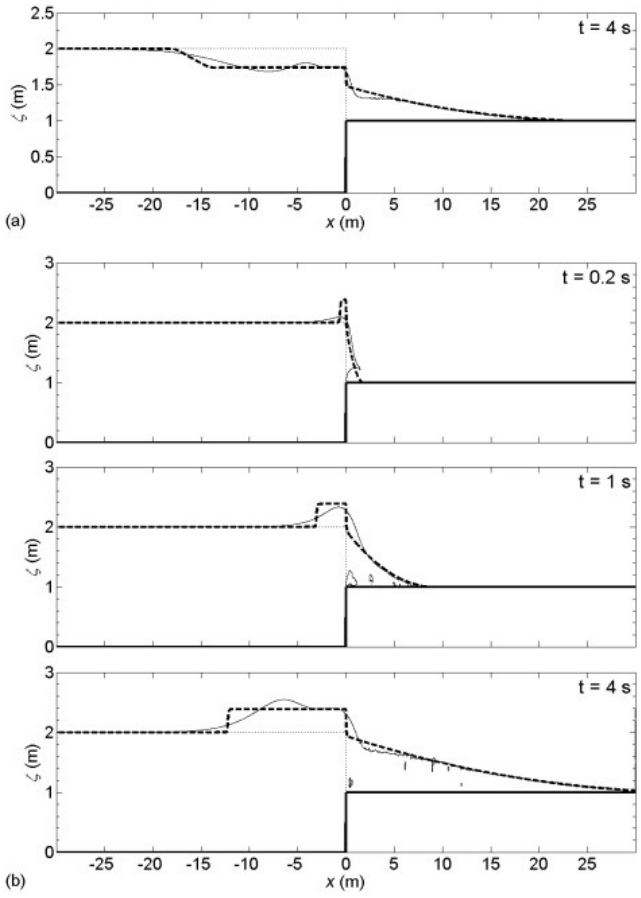

Figure 3. Reflection and overwash of a discontinuous flow onto a dry bed. (a) U_L = 0. (b) U_L = 2 m/s. The dotted, dash, and solid lines denote the initial surface elevation, depth-integrated model, and OpenFOAM.

Figures 4a and 4b illustrate the results for the downstream processes involving free fall of water without and with an initial velocity. The depth-integrated model gives an accurate account of the rarefaction waves and thus the overtopping rates in both cases. The OpenFOAM results show more detailed processes including detachment of the waterfall from the wall. The impinging jet produces an unsteady air-water circulation by the step and a surge in the downstream direction. The depth-integrated model produces a steady flow from the step that gradually transitions into a surge. The source term in these cases does not physically translate to the hydrostatic force on the step as in the formulation of the HLLS Riemann solver, but rather provides a mechanism to account for the potential energy of the waterfall and its contribution to the momentum of the downstream flow. Although the formulation of the Riemann problem does not account for the waterfall, the depth-integrated model gives good qualitative agreement with OpenFOAM for the resulting surge.

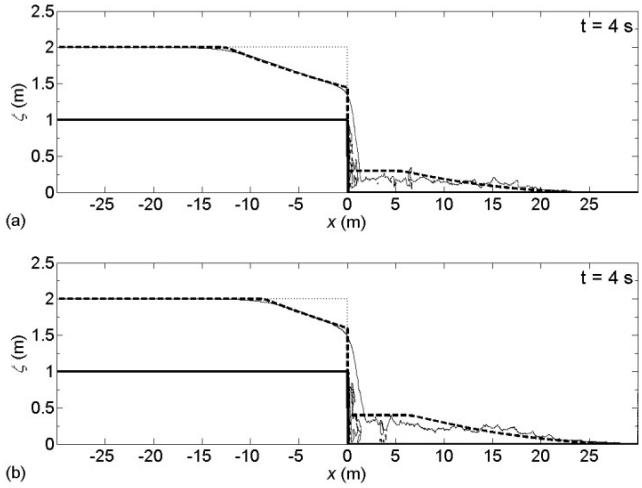

Figure 4. Free fall of a discontinuous flow onto dry bed. (a) U_L = 0. (b) U_L = 2 m/s. The dotted, dash, and solid lines denote the initial surface elevation, depth-integrated model, and OpenFOAM.

The computations were performed on an Intel I-7 processor for an elapsed time of 4 to 5 sec before the characteristic flows reach the boundaries. The time step is determined from a Courant number of 0.5 for the depth-integrated model and dynamically within OpenFOAM to maintain a stable solution. OpenFOAM was compiled and executed in the serial mode to compare with the computing time from the depth-integrated model. OpenFOAM takes approximately 8 hr for a 5 sec simulation, while the depth-integrated model can complete the calculation with less than 4 min in the Matlab environment. The computational cost of OpenFOAM will be substantially higher if a turbulence model is included. Although the computing time depends on many factors that vary between the two models and their operating environments, the results provide a general indication of the relative computational requirements. The depth-integrated model provides a highly efficient solution to the overtopping problem if only the characteristic flow patterns are of interest.

5. Laboratory Experiment

The laboratory experiment provided measurements of the reflection and transmission as well as the mixing processes from overtopping of a vertical structure by solitary waves. The collected data allows validation of the HLLS Riemann solver implemented in the depth-integrated model. Figure 5 illustrates the setup of the laboratory experiment at the Hydraulic Laboratory of the Department of Civil and Environmental Engineering, University of Hawaii.

The flume is 9.14 m long, 0.1524 m wide, and 0.39 m high with clear acrylic walls. The structure is 0.0762 m wide and 0.1524 m tall made from clear acrylic. A piston-type wavemaker generates

the incident solitary wave, which allows precise measurements of the flow characteristics for model validation (e.g., Roeber and Cheung, 2012; Quiroga and Cheung, 2013). The incident wave height a is measured from the still-water level. Three capacitance-type wave gauges sample the surface elevations at 76 Hz with an uncertainty of 5×10^{-5} m. Gauge 1 in front of the structure provides measurements of the incident and reflected waves. Gauge 2 just outside the downstream mixing zone captures the regenerated waves, while gauge 3 records the downstream flow. The wave gauges are connected to a data acquisition system controlled by the WinLabEM software.

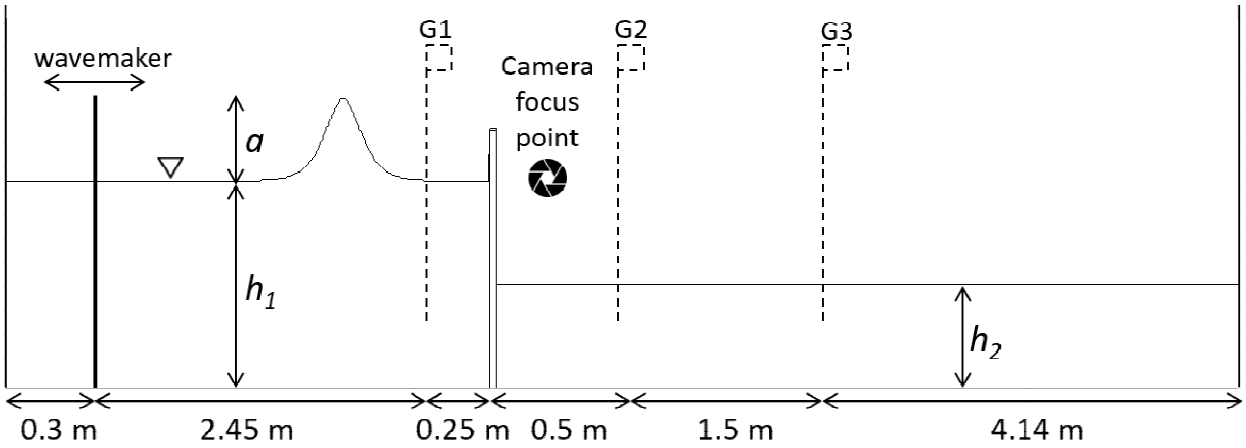

Figure 5. Setup of the laboratory flume experiment.

The clear acrylic flume allows illumination of the air-water interface with LED lights placed underneath and provides unobstructed views of the flow during the experiment. A high-speed camera with a Nikkor 50mm f/1.8D lens captures the overtopping and mixing processes at 400 fps. The camera is placed at 2 m from the wave flume, at an elevation of 0.12192 m above the bottom, and a distance of 0.22 m downstream of the structure. The MATLAB Image Processing Toolbox allows refinement of the image contrast and extraction of the surface profile on the front face of the flume for comparison with the model results. The post-processing of the high-speed video data includes correction for lens distortion and parallax error as well as mapping of pixel coordinates to real-world coordinates (Brady et al., 2004). The error is greatest near the edges of view and is much smaller at the image directly in front of the camera, where overtopping occurs. The post-processed images, which have been cropped accordingly, allow examination of the mixing processes and their effects on wave regeneration in comparison with the depth-integrated model results.

6. Model Validation

The depth-integrated model covers a flume of 10 m long with the structure located at the center to reproduce the laboratory test conditions. The one-dimensional model accounts for the front and back walls of the structure as opposing steps connected by computational cells along the crest. The incident solitary wave is defined as part of the initial conditions. Because a solitary wave has an infinite wavelength in theory, it is necessary to truncate its tails for the finite computational domain. The initial wave is positioned along the flume such that the surface elevation at the structure is less than 1% of the wave height. Numerical dispersion, which

depends on the spatial discretization as indicated in Section 2, is needed to maintain the incident solitary wave profile in lieu of the dispersion terms in the governing equation (1). The grid size on the upstream side requires a large value to provide sufficient dispersion for the given water depth (Yoon et al., 2007), but is limited to 4.5 cm for resolution of the wave processes. The structure and the downstream side have a finer grid of 9.5 mm to resolve shock-related hydraulic processes. A Manning number of 0.009 s/m$^{1/3}$ is used to account for the friction on the acrylic surface. An open boundary condition is imposed at both ends of the computational domain.

The laboratory experiments provided important data to validate the HLLS Riemann solver for modeling of wave overtopping. Figure 6 compares the results for a baseline test case with the same water depth on both sides equal to the height of the structure and the incident wave condition of $a/h_1 = 0.3$. The overtopping does not produce splashing or air entrainment in the downstream flow that violates the basic structure of a depth-integrated flow. At gauge 1 in front of the structure, the model provides a good depiction of the incident wave profile. The larger and more abrupt reflection from the front wall, as indicated by the second peak, results from the HLLS Riemann solver, in which the shock approximation overestimates the reflected wave height under transient conditions (See Figure 3 and associated discussion). The incident wave subsequently transforms into a surge on the structure that in turn transitions from supercritical to subcritical across the back wall. The video image shows good overall agreement of the model results with the measurements except near the structure, where the actual transition of the flow regime is more gradual and further downstream due to formation of a submerged jet above initially stagnant water. Gauges 2 recorded a transient initial pulse generated by the submerged jet and surface disturbances associated with unsteady circulations in the mixing zone. The measurements at gauge 3 show a well-developed solitary wave followed by trailing oscillations with diminishing amplitude. The model produces a solitary wave of comparable amplitude and phase but with steepened front face due to the absence of dispersion terms in the governing equation.

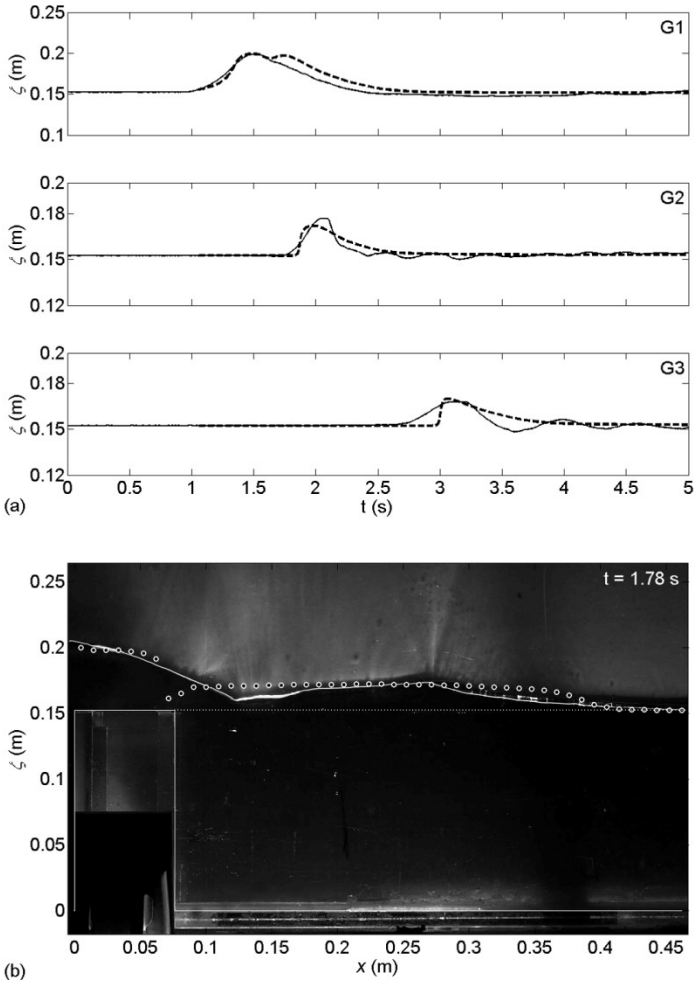

Figure 6. Comparison of numerical and laboratory results for wave overtopping. (a) Computed (dash line) and recorded (solid line) surface elevation time series at wave gauges. (b) Recorded image and computed surface profile (white circles). The water surface in the recorded image is highlighted as needed for ease of comparison. The dotted line indicates the initial surface elevation.

The CFD experiments have already shown the capability of the HLLS Riemann solver in describing complex flows generated by a waterfall. Figure 7 shows one of the more critical test cases with formation of a water jet in the air from the overtopping. The downstream water depth is half of the structure height. The smaller incident wave height of a/h_1 = 0.2 produces a longer solitary wave and a more enduring flow from the water jet. The model results at gauge 1 are not sensitive to the downstream flow and are similar to those in the first example. The video image shows a jet from the structure impinging the water surface with significant air entrainment. Gauge 2 recorded a large leading wave followed by surface disturbances generated by the mixing processes, while the measurements at gauge 3 show a distinct solitary wave. The model gives a reasonable description of the wave generation through potential energy release from the jet, but underestimates the amplitude and speed of the downstream solitary wave in comparison with the gauge measurements. A review of the remaining 28 tests shows the model has better performance for smaller amplitude and longer waves supporting the use of the HLLS Riemann solver. However, the discrepancies in the upstream reflected wave height and downstream propagation speed remain in most of the tests. These are related to the circulation in front of the structure and the impinging jet in the mixing zone that are not amenable to the depth-integrated approach.

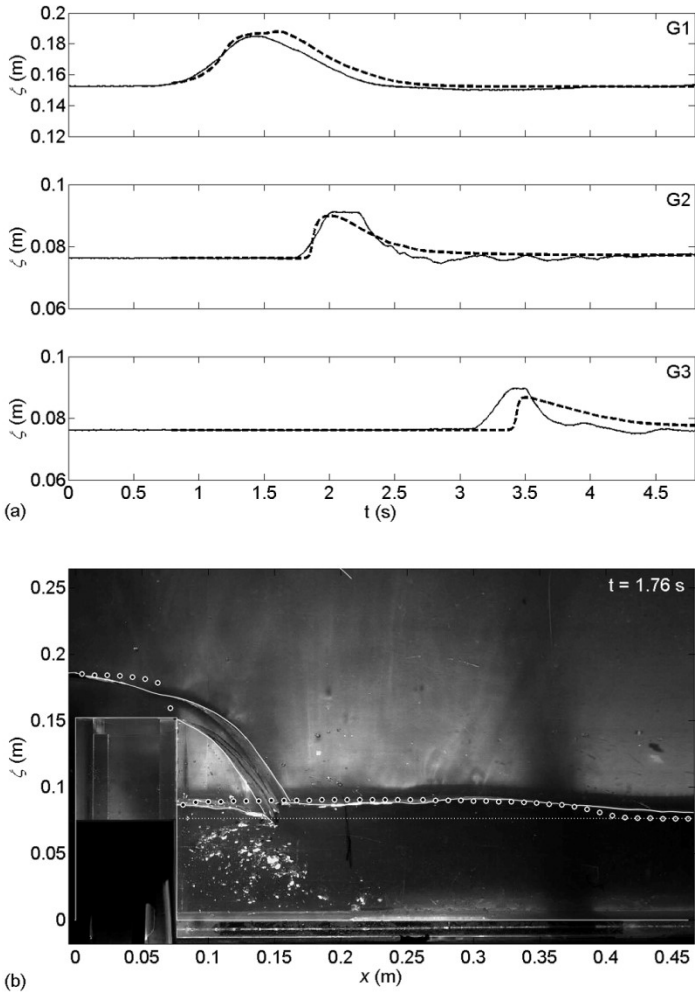

Figure 7. Comparison of numerical and laboratory results for jet formation. (a) Computed (dash line) and recorded (solid line) surface elevation time series at wave gauges. (b) Recorded image and computed surface profile (white circles). The water surface in the recorded image is highlighted as needed for ease of comparison. The dotted line indicates the initial surface elevation.

The HLLS Riemann solver, which incorporates effects of a bottom step in the source term, has proved both efficacious and efficient in modeling of free surface flow over a structure. This rather simple approach can greatly enhance the use of the depth-integrated approach for modeling of coastal wave processes. This opens up many research opportunities for further research in coastal wave modeling. Similar extension can be made to a non-hydrostatic or Boussinesq model to include effects of wave dispersion. However, precautions are deemed necessary in the interpretation of the model results due to the hydrostatic approximation of the source term, the shock assumption of the middle state, and the depth-integrated flow structure in

the solver. Some of these issues can be resolved by the use of an exact Riemann solver, which requires additional constraints to define a unique solution (e.g., Alcrudo and Benkhaldoun, 2001; Bernetti et al., 2008). Additional CFD and large-scale laboratory tests are necessary to evaluate and identify empirical processes that help calibrate the solver beyond its hydrostatic assumptions.

7. Training and Education

An important part of the project was to provide training, research opportunities, and financial support to graduate students in the Department of Ocean and Resources Engineering at the University of Hawaii. There are well-qualified admission applicants, but the number of students enroll in the program primarily depends on the available research assistantships. The following is a list of graduate students, who received support from ONR Grant N00014-12-1-0721, and their current employment:

1. Morgan A. Stephenson (MS 2015), Coastal Engineer, Sea Engineering Inc., Honolulu, Hawaii.
2. Matthew J. Wesley (MS 2015), Coastal Engineer, US Army Corps of Engineers, Los Angeles District, California.
3. Troy W. Heitmann, PhD Candidate in Ocean and Resources Engineering, University of Hawaii, Honolulu, Hawaii.

They have produced quality research work suitable for publication in refereed journals and international conference proceedings. Both MS graduates are working in an increasingly important engineering field in the US and around the world. Troy Heitmann, who is currently wrapping up his PhD dissertation, will graduate in the summer of 2017. He plans to continue his research and obtain a faculty position in the near future.

8. Concluding Remarks

The research project has advanced our understanding on a number of issues related to coastal wave modeling. These include development of a numerical dispersion relation defining the amplitude and phase errors from the sampling intervals in time and space as well as an extension of depth-integrated models to account for three-dimensional effects of wave overtopping. Scientists and engineers currently rely on numerical experiments to estimate model errors or use their experience to determine the required resolution in the model setup. The numerical dispersion relation replaces this empirical approach by quantifying effects of discretization on the numerical results. The extension of depth-integrated models to account for wave overtopping greatly enhances the model capability in describing complex flow patterns in the littorals and provides reliable results for practical application.

The analytical and numerical tools developed in this study have enhanced the capability to model the operating and design environments for vessels in the littorals. Concurrent ONR projects are investigating the use of CFD codes, such as CFDShip-Iowa, LS-DYNA, and OpenFOAM (NavyFOAM), for modeling of ship loads and motions. A systematic, nested-grid approach can link coastal wave and CFD modeling to produce a realistic, virtual coastal environment for seakeeping analysis.

References

Abbott, M.B. (1976). Computational hydraulics: a short pathology. *Journal of Hydraulic Research*, 14(4), 271-285.

Alcrudo, F. and Benkhaldoun, F. (2001). Exact solution to the Riemann problem of the shallow water equations with discontinuous bottom geometry. *Computers and Fluids*, 30(6), 634-671.

Brady, P.D.M., Boutounet, M., and Beecham, S. (2004). Free surface monitoring using image processing. *Proceedings of 15th Australasian Fluid Mechanics Conference*, Sydney, Australia.

Bernetti, R., Titarev, V.A., and Toro, E.F. (2008). Exact solution of the Riemann problem for the shallow water equations with discontinuous bottom geometry. *Journal of Computational Physics*, 227(6), 3212-3243.

Fuhrman, D.R. and Madsen, P.A. (2009). Tsunami generation, propagation, and run-up with a higher order Boussinesq model. *Coastal Engineering* 56 (7), 747–758.

George, D.L. (2008). Augmented Riemann solvers for the shallow water equations over variable topography with steady states and inundation. *Journal of Computational Physics*, 227(6), 3089-3113.

George, D.L. (2011). Adaptive finite volume methods with well-balanced Riemann solvers for modeling floods in rugged terrain: Application to the Malpasset dam-break flood. *International journal for Numerical Methods in Fluids*, 66(8), 1000-1018.

Gobbi, M.F., Kirby, J.T., Wei, G. (2000). A fully nonlinear Boussinesq model for surface waves. Part 2. Extension to O(kh)^4. *Journal of Fluid Mechanics* 405, 181-210.

Heitmann, T., Bai, Y., Cheung, K.F., Roeber, V. (2015). Dispersion preserving numerical schemes for coastal wave propagation. *International Workshop on the Application of Fluid Mechanics to Disaster Reduction*, Sendai, Japan.

Imamura, F., Shuto, N., and Goto, C. (1988). Numerical simulation of the transoceanic propagation of tsunamis. *Sixth Congress of the Asian and Pacific Division of the International Association for Hydraulic Research*, Kyoto, Japan.

Madsen, P.A., Murray, R., and Sørensen, O.R. (1991). A new form of Boussinesq equations with improved linear dispersion characteristics. *Coastal Engineering*, 15(4), 371-388.

Madsen, P.A. and Schäffer, H.A. (1998). Higher order Boussinesq-type equations for surface gravity waves-Derivation and analysis. *Philosophical Transactions of the Royal Society of London*, A 356, 3123-3186.

Murillo, J. and Garcia-Navarro, P. (2010). Weak solutions for partial differential equations with source terms: Application to the shallow water equations. *Journal of Computational Physics,* 229, 4327-4368.

Murillo, J. and Garcia-Navarro, P. (2012). Augmented versions of the HLL and HLLC Riemann solvers including source terms in one and two dimensions for shallow flow applications. *Journal of Computational Physics,* 231, 6861-6906.

Nwogu, O. (1993). An alternative form of the Boussinesq equations for nearshore wave propagation. *Journal of Waterway, Port, Coastal, and Ocean Engineering* 119 (6), 618-638.

Peregrine, D.H. (1967). Long waves on a beach. *Journal of Fluid Mechanics*, 27, 815-827.

Quiroga, P.D. and Cheung, K.F. (2013). Laboratory study of solitary wave transformation over bed-form roughness on fringing reefs. *Coastal Engineering*, 80, 35-48.

Roeber, V. and Cheung, K.F. (2012). Boussinesq-type model for energetic breaking waves in fringing reef environment. *Coastal Engineering*, 70, 1-20.

Roeber, V., Cheung, K.F., and Kobayashi, M.H. (2010). Shock-capturing Boussinesq-type model for nearshore wave processes. *Coastal Engineering*, 57(4), 407-423.

Stephenson, M.A. (2015). Implementation of CMS for Fringing Reef Environments. MS Paper, University of Hawaii, Honolulu.

Tam, C.K.W. and Webb, J.C. (1993). Dispersion relation preserving finite difference schemes for computational acoustics. *Journal of Computational Physics*, 107(2), 261-281.

Wei, G., Kirby, J.T., Grilli, S.T., and Subramanya R. (1995). A fully nonlinear Boussinesq model for surface waves: Part I. Highly nonlinear unsteady waves. *Journal of Fluid Mechanics*, 294, 71-92.

Wesley, M.J. (2015). Bottom-discontinuous Riemann Solver for Modeling of Wave Overtopping. MS Thesis, University of Hawaii, Honolulu.

Wesley, M.J. and Cheung, K.F. (2016). Modeling of wave overtopping on vertical structures with the HLLS Riemann solver. *Coastal Engineering*, 112, 28-43.

Wang, X. and Liu, P.L.-F. (2011). An explicit finite difference model for simulating weakly nonlinear and weakly dispersive waves over slowly varying water depth. *Coastal Engineering*, 58, 173-183.

Weller, H.G., Tabor, G., Jasak, H., and Fureby, C. (1998). A tonsorial approach to computational continuum mechanics using object oriented techniques. *Computers in Physics*, 12(6), 620-631.

Yoon, S.B., Lim, C.H., Choi, J. (2007). Dispersion-correction finite difference model for simulation of transoceanic tsunamis. *Terrestrial, Atmospheric and Oceanic Sciences*, 18(1), 31-53.

Zhou, J.G., Causon, D.M., Ingram, D.M., and Mingham, C.G. (2001). The surface gradient method for the treatment of source terms in the shallow-water equations. *Journal of Computational Physics*, 168(1),